Tailoring the Solid-State Fluorescence of BODIPY by Supramolecular Assembly with Polyoxometalates

Patricia Bolle, Tarik Benali, Clotilde Menet, Marin Puget, Eric Faulques, Jérôme Marrot, Pierre Mialane, Anne Dolbecq, Hélène Serier-Brault, Olivier Oms, et al.

Tailoring the Solid-state Fluorescence of BODIPY by Supramolecular Assembly with Polyoxometalates

Patricia Bolle,[a] Tarik Benali,[b] Clotilde Menet,[a] Marin Puget,[a] Eric Faulques,[a] Jérome Marrot,[b] Pierre Mialane,[b] Anne Dolbecq,[b] Hélène Serier-Brault,[a] Olivier Oms,[b]* and Rémi Dessapt[a]*

[a]Université de Nantes, CNRS, Institut des Matériaux Jean Rouxel, IMN, F-44000 Nantes, France

[b]Université Paris-Saclay, UVSQ, CNRS, Institut Lavoisier de Versailles, 78000, Versailles, France

ABSTRACT: A cationic boron dipyrromethene (BODIPY) derivative ($\mathbf{1}^+$) has been successfully combined with two polyoxometalates (POMs), the Lindqvist-type $[W_6O_{19}]^{2-}$ and the β-$[Mo_8O_{26}]^{4-}$ units, into three new supramolecular fluorescent materials $\mathbf{(1)_2[W_6O_{19}]\cdot 2CH_3CN}$, $\mathbf{(1)_2[W_6O_{19}]}$ and $\mathbf{(1)_4[Mo_8O_{26}]\cdot DMF\cdot H_2O}$. The resulting hybrid compounds have been fully characterized by a combination of single-crystal X-ray diffraction, IR and UV-Vis spectroscopies and photoluminescence analyses. This self-assembly approach prevents any π-π stacking interactions between the BODIPY units, responsible for aggregation-caused quenching (ACQ) effects, but also between the BODIPY and the POMs, avoiding intermolecular charge-transfer effects. Noticeably, the POM units do not only act as bulky spacers but their negative charge density drives the molecular arrangement of the $\mathbf{1}^+$ luminophore, strongly modifying its fluorescence in the solid state. As a consequence, the $\mathbf{1}^+$ cations are organized into dimers in $\mathbf{(1)_2[W_6O_{19}]\cdot 2CH_3CN}$ and $\mathbf{(1)_2[W_6O_{19}]}$, which are weakly emissive at room temperature, and in a more compact layered assembly in $\mathbf{(1)_4[Mo_8O_{26}]\cdot DMF\cdot H_2O}$ which exhibits a red-shifted and intense emission upon similar photoexcitation.

1. INTRODUCTION

The interest for organic solid-state luminescent materials has greatly increased in the last decade. Integrated in optoelectronic devices,[1] they found applications in various fields such as lasers,[2] organic light-emitting diodes (OLEDs),[3] sensors,[4] bioimaging[5] or anti-counterfeiting technologies.[6] Despite their high photostability and fluorescent quantum yields along with narrow emission bands, the well-known class of boron dipyrromethene (BODIPY)[7] fluorophores has been intensively investigated almost exclusively for their use in diluted solutions. Actually, in the condensed phase, the strong intermolecular π–stacking interactions between these aromatic planar dyes lead to aggregation-caused quenching (ACQ) effects, thus limiting their integration in efficient optical devices. To overcome this specific issue, several strategies have been reported up to now (Table S1). First, due to the great chemical versatility of this family of compounds, it is possible either to functionalize the BODIPY skeleton by bulky substituents that inhibit the aggregation of the chromophores,[8–11] or to synthesize specific dyes that are structurally arranged into emissive aggregates, exhibiting the well-known aggregation-induced enhanced emission (AIE) behavior.[12–17] A second strategy which avoids numerous time-consuming synthetic steps consists in the dilution of the BODIPY molecules into matrices. So, it has been demonstrated that the incorporation of the fluorophore into a polymer matrix diminishes the formation of non-emissive aggregates.[18–20] In the same way and following an elegant synthetic route, it has been recently shown that the entrapment of commercial BODIPY derivatives into a Metal-Organic Framework (MOF) strongly enhanced their solid-state luminescence.[21] However, in addition to the problem of long-term chemical stability, it remains difficult via this method to finely control the substrate organization in the MOF pores, and in absence of single-crystal X-ray diffraction characterizations, an accurate structural description of such chromophore@MOF composites remains difficult, hindering structure/property correlations.

In the last decade, we have shown that the combination of polyoxometalates (POMs), which can be described as anionic soluble metal oxides of early transition metals (usually W, Mo, V),[22–24] with photoactive organic or organometallic species strongly tunes their optical properties. As a striking example, while they exhibit poor solid-state photochromism properties at room temperature, pure organic spiropyran and spironaphthoxazine derivatives became highly photoactive when closely associated to POMs through ionic or covalent bonds.[25–29] Recently, ionic supramolecular assemblies have been easily built by mixing different polyoxoanions and a luminescent cationic cyclometalated Ir(III) complex.[30,31] Remarkably, the solid-state emission of the resulting compounds shifts from green to red depending on the nature of the POM and the crystal packing. Moreover, some of us recently designed novel supramolecular fluorescent materials by coupling POMs with an AIE-active phospholium,[32] and efficient solid-state emitters have been obtained by directing favorably the balance between AIE and ACQ effects using both anion-π^+ and H-bonding interactions. In view of these significant results, we decided to enlarge our strategy to BODIPY entities with the hope to recover their outstanding physico-chemical properties in the solid state in a simple and controlled way. To date, very scarce examples of BODIPY/POM dyads have been mentioned in the literature, and in most of the cases, the organic and inorganic fragments have been linked through covalent bonds.[33–36'] We can mention the synthesis in 2015 of a molecular fluorescent photoswitch obtained by combining in a single molecule an Anderson-type POM, a spiropyran group and a BODIPY moiety.[34] Very recently, two supramolecular assemblies of a cationic iodobodipy and polyoxovanadates have been elaborated for photochemotherapy in solution.[37] However, to the best of our knowledge, the solid-state photophysical properties of such ionic or covalent hybrid systems remained uninvestigated.

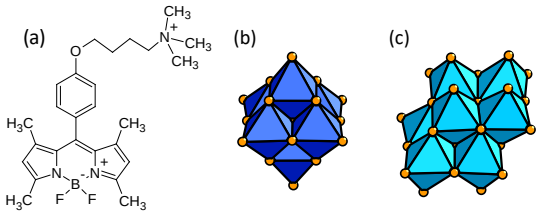

Figure 1. Representations of (a) the cationic BODIPY (**1**$^+$), (b) the $[W_6O_{19}]^{2-}$ and (c) the β-$[Mo_8O_{26}]^{4-}$ units considered in this study (dark blue octahedra = WO_6, light-blue octahedra = MoO_6, gold sphere: oxygen).

We report herein the straightforward synthesis of three crystallographically resolved POM/BODIPY supramolecular assemblies, obtained by combining octamolybdate or Lindqvist-type tungsten polyanions and a cationic BODIPY derivative[38] (denoted as **1**$^+$), displayed in Figure 1. The solid-state photophysical properties at room temperature of the reported hybrids, namely **(1)$_2$[W$_6$O$_{19}$]·2CH$_3$CN**, **(1)$_2$[W$_6$O$_{19}$]** and **(1)$_4$[Mo$_8$O$_{26}$]·DMF·H$_2$O** have been thoroughly investigated and pertinent structure-property relationships have been evidenced. As envisaged, the structural analysis well indicates the absence of undesired π–π stacking interactions between the BODIPY cations likely to induce non-emissive aggregates. Moreover, we emphasize the essential role of the POM onto the emission of the cationic fluorophore in the crystalline state.

2- EXPERIMENTAL SECTION

2.1. Synthetic procedures. All chemicals and reagents were purchased from major chemical suppliers and used as received except $(NBu_4)_4[\alpha\text{-}Mo_8O_{26}]$[39] and $(NBu_4)_2[W_6O_{19}]$[40] which have been synthesized according to the reported procedures. $((CH_3CH_2)_2NH_2)_2(NH_4)_2[Mo_8O_{26}]$, which was used as an optical reference of the β-$[Mo_8O_{26}]^{4-}$ unit for solid-state UV-vis spectroscopy characterizations, was also synthesized as previously described.[41]

2.1.1. Synthesis of 4,4-Difluoro-8-(4-(4-(N,N,N-trimethyl)aminobutoxy))phenyl-1,3,5,7-tetramethyl-4-bora-3a,4a-diaza-s-indacene bromide (**(1)Br**). **(1)Br** has been prepared by a slight modification of the previously reported procedure,[38] according to the synthetic pathway displayed in the Supporting Information.

2.1.2. Synthesis of **(1)$_2$[W$_6$O$_{19}$]·2CH$_3$CN** and **(1)$_2$[W$_6$O$_{19}$]**. $(NBu_4)_2[W_6O_{19}]$ (0.0889 g, 4.70 10^{-2} mmol) was dissolved in acetonitrile (3 mL). The colourless solution (solution 1) was stirred for a few minutes at room temperature. Meanwhile, a second solution (solution 2) was obtained by dissolving **(1)Br** (0.050 g, 9.36 10^{-2} mmol) in acetonitrile (2 mL) at room temperature. Solution 2 was added dropwise to solution 1 under vigorous stirring and the resulting reddish-brown solution was heated at 40 °C for two hours, the precipitation of an orange powder being observed from the beginning of heating. The mixture was kept at room temperature and then filtered. Orange-red single crystals of **(1)$_2$[W$_6$O$_{19}$]·2CH$_3$CN** were obtained after a few days by slow diffusion of *tert*-butyl methyl ether into the filtrate. Yield in W: 38%. Anal. Calcd for $C_{56}H_{76}B_2F_4N_8O_{21}W_6$: C, 28.03 ; H, 3.16 ; N, 4.67. Found: C, 28.69 ; H, 3.52 ; N, 4.67. FT-IR (KBr cm^{-1}): **1**$^+$ cation 1609 (w), 1545 (m), 1508 (w), 1470 (m), 1408 (w), 1379 (w), 1363 (w), 1306 (m), 1286 (w), 1246 (m), 1196 (m), 1157 (m), 1118 (w), 1086 (w), 1070 (w), 706 (w), 478 (w); νW=O, νW-O-W 976 (vs), 814 (vs), 766 (w), 586 (m), 445 (s).

The obtained orange powder which had first precipitated was washed with ethanol, dried in air and dissolved in DMF (4 mL). The resulting solution was stirred at 50 °C for 1 h, and the system was set to standby at ambient temperature. Orange-red single crystals of **(1)$_2$[W$_6$O$_{19}$]** were obtained after a few days. Yield in W: 34%. Anal. Calcd for $C_{52}H_{70}B_2F_4N_6O_{21}W_6$: C, 26.97 ; H, 3.05 ; N, 3.63. Found: C, 27.41 ; H, 2.96 ; N, 3.49. FT-IR (KBr cm^{-1}): **1**$^+$ cation 1610 (w), 1545 (m), 1508 (w), 1472 (m), 1406 (w), 1371 (w), 1306 (m), 1286 (w), 1250 (m), 1194 (m), 1155 (m), 1120 (w), 1084 (w), 704 (w), 476 (w); νW=O, νW-O-W 976 (vs), 812 (vs), 764 (w), 584 (m), 444 (s).

2.1.3. Synthesis of **(1)$_4$[Mo$_8$O$_{26}$]·DMF·H$_2$O**. $(NBu_4)_4[\alpha\text{-}Mo_8O_{26}]$ (0.050 g, 2.32 10^{-2} mmol) was dissolved in acetonitrile (3 mL). The colourless solution (solution 1) was stirred for a few minutes at room temperature. Meanwhile, a second solution (solution 2) was obtained by dissolving **(1)Br** (0.050 g, 9.36 10^{-2} mmol) in acetonitrile (3 mL) at room temperature. Solution 2 was added dropwise to solution 1 under vigorous stirring and the resulting reddish-brown solution was heated at 40 °C for two hours leading to the precipitation of a reddish-orange solid. The mixture was kept at room temperature and then filtered. The powder was washed with ethanol, and dried in air. Then the powder was dissolved in DMF (4 mL). The resulting solution was stirred at 50 °C for 1 h, and the system was set to standby at ambient temperature. Red single crystals were obtained after a few days. Yield in Mo: 32%. Anal. Calcd for $C_{107}H_{149}B_4F_8Mo_8N_{13}O_{32}$: C, 41.54; H, 4.82 ; N, 5.89. Found: C, 42.23 ; H, 4.54 ; N, 6.69. FT-IR (KBr cm^{-1}): **1**$^+$ cation 1610 (w), 1545 (m), 1508 (w), 1472 (m), 1406 (w), 1371 (w), 1306 (m), 1286 (w), 1250 (m), 1194 (m), 1155 (m), 1120 (w), 1084 (w), 1151 (w), 704 (w), 476 (w); νMo=O, νMo-O-Mo 976 (vs), 812 (vs), 764 (w), 584 (m), 444 (s).

3. RESULTS AND DISCUSSION

3.1. Synthesis. (1)Br was prepared in a three-step synthetic procedure via a slight modification of the previously reported protocol.[38] ^{1}H (Figure S1) and ^{13}C NMR spectroscopies as well as mass spectrometry data (Figure S2) confirmed the formation of the product, which was isolated as a reddish-brown powder. Unfortunately, attempts to obtain single crystals were unsuccessful. Orange-red single crystals of **(1)$_2$[W$_6$O$_{19}$]** were isolated by recrystallization in DMF at room temperature of the orange powder obtained by mixing in acetonitrile $(NBu_4)_2[W_6O_{19}]$ and two equivalents of **(1)Br**. In addition, orange-red single crystals of **(1)$_2$[W$_6$O$_{19}$]·2CH$_3$CN** were obtained by slow diffusion of *tert*-butyl methyl ether into the acetonitrile filtrate of the same **(1)Br**/$[W_6O_{19}]^{2-}$ mixture. FT-IR spectroscopy (Figures S3-S4) well evidences that both compounds contain the $[W_6O_{19}]^{2-}$ anion associated with **1**$^+$ cations. The presence of crystallized acetonitrile molecules in **(1)$_2$[W$_6$O$_{19}$]·2CH$_3$CN** has been also confirmed by elemental analyses and thermogravimetric analysis (Figure S5). **(1)$_4$[Mo$_8$O$_{26}$]·DMF·H$_2$O** was obtained as red single crystals by mixing in acetonitrile $(NBu_4)_4[Mo_8O_{26}]$ and four equivalents of **(1)Br**, and after recrystallizing the resulting reddish-orange powder in DMF at room temperature. The presence of the β-$[Mo_8O_{26}]^{4-}$ unit and a co-crystallized DMF molecule

were confirmed by FT-IR spectroscopy (Figure S6). The presence of a co-crystallized water molecule, observed by X-ray diffraction data (see below), could be due to the presence of a small quantity of water in the organic solvents used or/and to moisture from air.

3.2 Structural Description. $(\mathbf{1})_2[W_6O_{19}]\cdot 2CH_3CN$. The crystal structure of $(\mathbf{1})_2[W_6O_{19}]\cdot 2CH_3CN$ contains two crystallographically equivalent $\mathbf{1}^+$ cations assembled with one $[W_6O_{19}]^{2-}$ unit into supramolecular $\{(\mathbf{1})_2[W_6O_{19}]\}$ ribbons running along the *a*-axis (Figure 2a). The polar alkylammonium groups of the $\mathbf{1}^+$ molecules interact via electrostatic interactions including C–H···O contacts with the oxygen POM surface, and the acetonitrile molecules are localized between $\mathbf{1}^+$ cations. In these latter, the *meso*-phenyl ring is almost orthogonal to the indacene plane with a dihedral angle of 81.19°. This conformation should minimize unfavorable steric hindrances between the ortho-hydrogen atoms and the vicinal methyl groups.[42] In addition, the butylammonium chain is in a folded conformation (Figure 2b), with a distance between the boron atom and the ammonium head group of 11.95 Å. In the $\{(\mathbf{1})_2[W_6O_{19}]\}$ ribbons, the boradiazaindacene groups form a columnar slipped stack along the *a*-axis. However, the POMs units keep the $\mathbf{1}^+$ molecules away from each other, inducing a long centre-to-centre distance of 9.586 Å between the aromatic planes. In addition, the $\{(\mathbf{1})_2[W_6O_{19}]\}$ ribbons are stacked along the *b*-axis (Figure S7). The methyl substituents of the pyrrole groups interact with the POM unit via weak C-H···O contacts which prevent any π-π stacking interactions with the oxygen POM surface likely to induce intermolecular charge transfer processes. Between two adjacent ribbons, the $\mathbf{1}^+$ molecules form isolated head-to-tail dimers with a distance between both indacene planes of 6.124 Å (Figure 2b). However, they are strongly offset from each other and interact through weak C-H···F and C-H···π hydrogen bonds, banishing any π-π stacking interactions. The dimers adopt a layered organization along the *ab* plane (Figure 2c), without any overlap of the aromatic planes of neighboring dimers. **$(\mathbf{1})_2[W_6O_{19}]$.** The crystal structure of $(\mathbf{1})_2[W_6O_{19}]$ contains two crystallographically inequivalent $\mathbf{1}^+$ conformers (hereafter labelled as 1^+_A and 1^+_B) which are assembled with the $[W_6O_{19}]^{2-}$ units in a herringbone-like pattern (Figure 3a), to form supramolecular ribbons running along the *a*-axis. These latter are then aligned parallel to form $\{(\mathbf{1})_2[W_6O_{19}]\}$ layers that are stacked along the *b*-axis (Figure S8).

Strikingly, the lack of crystallized solvent molecules in $(\mathbf{1})_2[W_6O_{19}]$ induces significant changes in the molecular crystal packing compared to that of $(\mathbf{1})_2[W_6O_{19}]\cdot 2CH_3CN$. In particular, the $\mathbf{1}^+$ volume concentration increases from 1.909×10^{-3} mol.cm^{-3} in $(\mathbf{1})_2[W_6O_{19}]\cdot 2CH_3CN$ to 1.978×10^{-3} mol.cm^{-3} in $(\mathbf{1})_2[W_6O_{19}]$. The conformation of the $\mathbf{1}^+$ molecules is also significantly modified. Indeed, while the angle between the *meso*-phenyl ring and the indacene plane (86.92° for 1^+_A and 75.3° for 1^+_B) is quite comparable with that observed in $(\mathbf{1})_2[W_6O_{19}]\cdot 2CH_3CN$ (81.19°), the butylammonium chain is in a long unfolded conformation this time, which increases the length of the BODIPY molecules, the distance between the boron atom and the ammonium head group reaching 14.25 Å for 1^+_A and 14.12 Å for 1^+_B (11.95 Å in $(\mathbf{1})_2[W_6O_{19}]\cdot 2CH_3CN$).

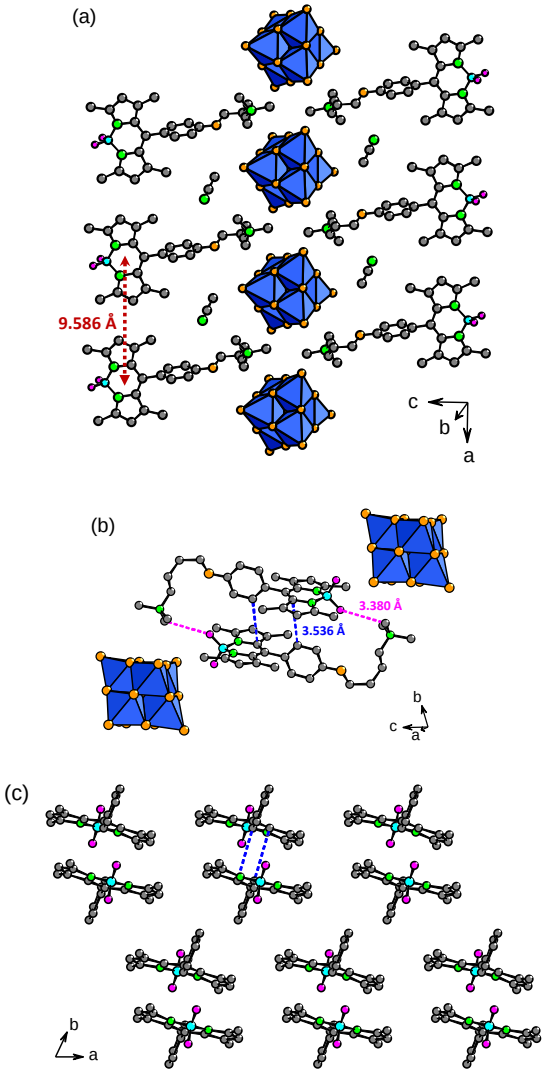

Figure 2. (a) Crystal packing diagram in $(\mathbf{1})_2[W_6O_{19}]\cdot 2CH_3CN$. (b) Supramolecular $\mathbf{1}^+$ dimer. (c) Molecular packing of the $\mathbf{1}^+$ dimers (ether groups are not displayed). Intermolecular C-H···π and C-H···F interactions are displayed as blue and pink dotted lines, respectively (dark blue octahedra = WO_6, gold sphere: oxygen, pink sphere: fluoride, blue sphere: boron, green sphere: nitrogen, grey sphere: carbon. H-atoms are omitted for clarity).

In the supramolecular $\{(\mathbf{1})_2[W_6O_{19}]\}$ layers, the $\mathbf{1}^+$ molecules are organized into columnar slipped stacks along the *a*-axis. However, due to the presence of the POM units, the shortest distances between the indacene planes are all over 9 Å (Figure 3b), and they mainly interact through intermolecular C-H···F hydrogen bonds implying the methyl substituents of the pyrrole groups. Moreover, the indacene planes do not interact with the oxygen POM facets via π-π stacking interactions. Along the *c*-axis, each $\mathbf{1}^+$ conformer is arranged into a head-to-tail dimer (Figure 3c) with a long centre-to-centre distance between the aromatic indacene planes of 7.322 Å for 1^+_A and 6.012 Å for 1^+_B. As observed for $(\mathbf{1})_2[W_6O_{19}]\cdot 2CH_3CN$, the neighboring indacene groups are mainly stabilized by intermolecular C-H···π contacts between the meso-phenyl ring and the pyrroles groups rather than π-π stacking interactions.

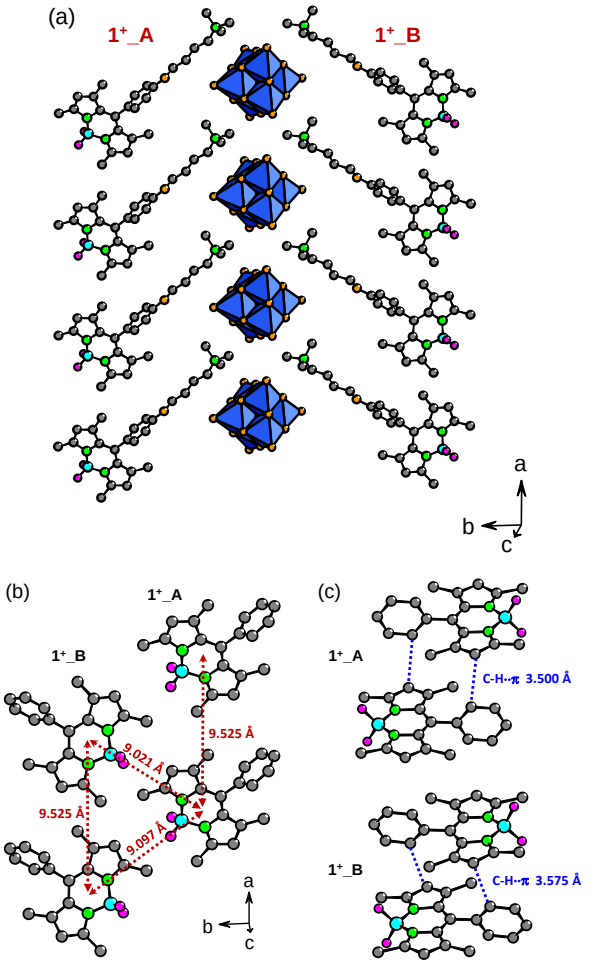

Figure 3. (a) Crystal packing diagram in $(\mathbf{1})_2[W_6O_{19}]$. Molecular arrangements of the $\mathbf{1}^+$ conformers (b) between two adjacent $\{(\mathbf{1})_2[W_6O_{19}]\}$ ribbons, and (c) into head-to-tail dimers (ether groups are not displayed). Intermolecular C-H···π interactions are displayed as blue dotted lines (dark blue octahedra = WO_6, gold sphere: oxygen, pink sphere: fluoride, blue sphere: boron, green sphere: nitrogen, grey sphere: carbon. H-atoms are omitted for clarity).

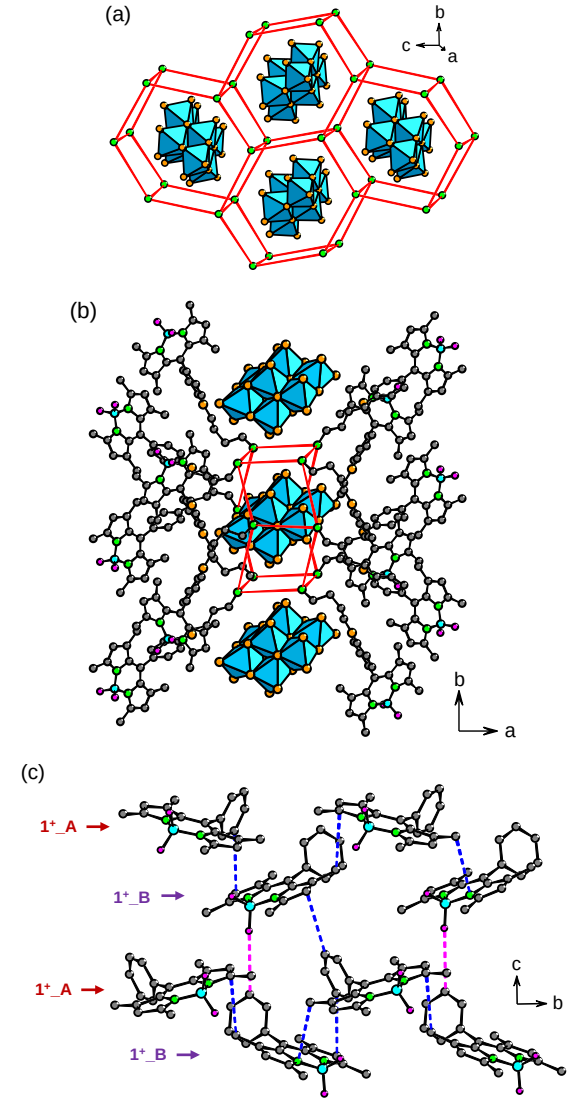

Figure 4. Crystal packing diagram in $(\mathbf{1})_4[Mo_8O_{26}]\cdot DMF\cdot H_2O$. (a) β-$[Mo_8O_{26}]^{4-}$ units in the wavy honeycomb-like supramolecular 2D network of $\mathbf{1}^+$ (only the N-atoms of the ammonium head groups are displayed). (b) Molecular packing of the $\mathbf{1}^+$ cations around the POM units. (c) Structural arrangement of the $\mathbf{1}^+$ conformers (ether groups are not displayed). Intermolecular C-H···π and C-H···F interactions are displayed as blue and pink dotted lines, respectively. (light blue octahedra = MoO_6, gold sphere: oxygen, pink sphere: fluoride, blue sphere: boron, green sphere: nitrogen, grey sphere: carbon. H-atoms are omitted for clarity).

$(\mathbf{1})_4[Mo_8O_{26}]\cdot DMF\cdot H_2O$. The crystal structure of $(\mathbf{1})_4[Mo_8O_{26}]\cdot DMF\cdot H_2O$ contains two crystallographically independent $\mathbf{1}^+$ cations (hereafter labelled as 1^+_A and 1^+_B), one β-$[Mo_8O_{26}]^{4-}$ unit, and DMF and water molecules. The ammonium head groups of the $\mathbf{1}^+$ cations form a wavy honeycomb-like supramolecular 2D network, and the POM clusters are localized inside the cavities (Figure 4a). Each β-$[Mo_8O_{26}]^{4-}$ unit is surrounded by twelve BODIPY molecules whom boradiazaindacene rings are oriented on both sides of the POM layer (Figure 4b and Figure S9). Four aromatic planes interact with the β-$[Mo_8O_{26}]^{4-}$ unit via C-H···O and short O···C contacts implying the *meso*-phenyl ring. The $\mathbf{1}^+$ volume concentration reaches 2.068×10^{-3} mol.cm^{-3} i.e., an increase of 4.5% and 8% compared to those determined for $(\mathbf{1})_2[W_6O_{19}]$ and $(\mathbf{1})_2[W_6O_{19}]\cdot 2CH_3CN$, respectively. Consequently, the boradiazaindacene cores of the two $\mathbf{1}^+$ conformers do not form supramolecular dimers as observed in $(\mathbf{1})_2[W_6O_{19}]$ and $(\mathbf{1})_2[W_6O_{19}]\cdot 2CH_3CN$, but they are alternately stacked in a layered arrangement along the (*bc*) plane, and mainly interact through a complex C-H···F and C-H···π hydrogen-bonding network (Figure 4c). The shortest centre-to-centre distance between the neighboring indacene planes is 6.523 Å, i.e. longer than the corresponding shortest distances in $(\mathbf{1})_2[W_6O_{19}]$ and $(\mathbf{1})_2[W_6O_{19}]\cdot 2CH_3CN$, and no π-π stacking interactions are observed.

3.3. Solid-state photophysical properties. The absorption and photoluminescence (PL) properties of **(1)Br** in diluted solution have been already investigated, indicating that $\mathbf{1}^+$ exhibits a green emission (λ_{em} = 511 nm) in 4-(2-hydroxyethyl)-1-piperazineethanesulfonic acid (HEPES) aqueous buffer.[38]

However, its photophysical properties in the solid state remain still unexplored. The room-temperature solid-state UV-vis absorption and steady-state PL spectra of **(1)Br** are depicted in Figure 5 and Figure S10. The intense absorption band at 460 nm could be attributed to vibrational bands of the strong $S_0 \rightarrow S_1$ (π-π^*) transition, while the less intense relatively broad band centered at 368 nm could correspond to the $S_0 \rightarrow S_2$ (π-π^*) transition. The weak absorption band at 538 nm could be assigned to intermolecular effects because it totally disappeared in diluted acetonitrile solution (Figure S11). 2D photoluminescence excitation-emission map (Figure S10) indicates that upon irradiation at λ_{ex} = 365 nm, **(1)Br** exhibits a weak fluorescence at room temperature. Its PL spectrum shows a broad and multimodal emission band in the 550-900 nm range with a wavelength maximum at 750 nm with six distinguishable shoulders peaking at 518, 550, 580, 632, 679 and 815 nm (Figure S10). A mean fluorescence lifetime of τ = 259 ps has been determined by room temperature time-resolved spectroscopy (Figure S12). This orange emission is characterized by the Commission Internationale de l'Eclairage (CIE) chromaticity coordinates of (0.58, 0.41) (Figure S13).

As expected, the solid-state emission of $\mathbf{1}^+$ is significantly red-shifted relative to the monomer in diluted solution[38] due to strong intermolecular interactions in the condensed state.[42-44] The weak emission of **(1)Br** suggests significant ACQ effects, as usually observed for BODIPY dyes free from bulky substituents grafted onto the boradiazaindacene group.

As shown in Figure 5, the solid-state UV-vis absorption spectra of $\mathbf{(1)_2[W_6O_{19}]\cdot 2CH_3CN}$, $\mathbf{(1)_2[W_6O_{19}]}$ and $\mathbf{(1)_4[Mo_8O_{26}]\cdot DMF\cdot H_2O}$ exhibit a weak overlap, limited to the 275–350 nm range, between the absorption bands of $\mathbf{1}^+$ and the O→M ligand-to metal charge-transfer (LMCT) transitions of the POM units (λ_{max} = 280 nm and 300 nm for the $[W_6O_{19}]^{2-}$ and β-$[Mo_8O_{26}]^{4-}$ anions, respectively). This well justifies the choice of these POMs whose high energy LMCT absorptions do not compete with the $\mathbf{1}^+$ photoexcitation upon 365-nm irradiation. In the 350-600 nm range, the spectra are indeed dominated by the intense absorption bands of $\mathbf{1}^+$.

The room-temperature steady-state PL excitation (PLE) spectra of the three hybrid POMs (Figure S14) show a broad band whom the maximum wavelength is located in the 350-400 nm range, in good agreement with the $S_0 \rightarrow S_2$ (π-π^*) transition of $\mathbf{1}^+$ observed in the absorption spectra of the three salts (Figure 5). The room-temperature steady-state emission spectra of $\mathbf{(1)_2[W_6O_{19}]\cdot 2CH_3CN}$, $\mathbf{(1)_2[W_6O_{19}]}$ and $\mathbf{(1)_4[Mo_8O_{26}]\cdot DMF\cdot H_2O}$ monitored at λ_{ex} = 365 nm are displayed in Figure 6.

As observed for **(1)Br**, $\mathbf{(1)_2[W_6O_{19}]\cdot 2CH_3CN}$ and $\mathbf{(1)_2[W_6O_{19}]}$ exhibit weakly intense orange fluorescence upon similar photoexcitation. The PL spectrum of $\mathbf{(1)_2[W_6O_{19}]\cdot 2CH_3CN}$ shows a broad and multimodal band centered at 678 nm. The PL profile of $\mathbf{(1)_2[W_6O_{19}]}$ is roughly comparable except the maximum wavelength which is shifted to 694 nm. These emissions are characterized by mean PL lifetimes of τ = 185 ps and 219 ps for $\mathbf{(1)_2[W_6O_{19}]\cdot 2CH_3CN}$ and $\mathbf{(1)_2[W_6O_{19}]}$, respectively (Figure S15).

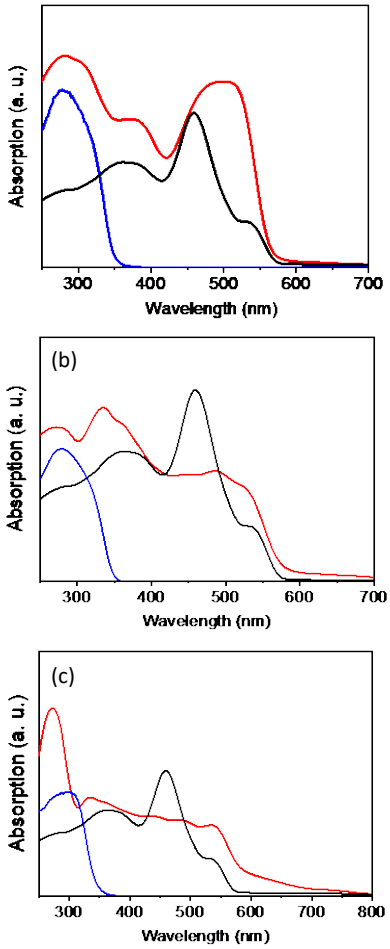

Figure 5. Solid-state UV-vis absorption spectra of (a), $\mathbf{(1)_2[W_6O_{19}]\cdot 2CH_3CN}$, (b) $\mathbf{(1)_2[W_6O_{19}]}$ and (c) $\mathbf{(1)_4[Mo_8O_{26}]\cdot DMF\cdot H_2O}$ (red lines), compared with those of **(1)Br** (black lines) and the optical POM references ($(NBu_4)_2[W_6O_{19}]$ or $((CH_3CH_2)_2NH_2)_2(NH_4)_2[Mo_8O_{26}]$) (blue lines).

In marked contrast, $\mathbf{(1)_4[Mo_8O_{26}]\cdot DMF\cdot H_2O}$ exhibits a bright orange-red emission (Figure 6, inset), much more intense than those of **(1)Br**, $\mathbf{(1)_2[W_6O_{19}]\cdot 2CH_3CN}$ and $\mathbf{(1)_2[W_6O_{19}]}$. Its PL spectrum displays a broad band peaking at 682 nm with a shoulder at 720 nm, and the mean PL lifetime reaches 0.39 ns, i.e. higher than those of the two polyoxotungstate species reported herein.

These results clearly highlight that the solid-state PL response of $\mathbf{1}^+$ can be tuned with the nature of the associated POM and the crystal packing. As envisaged, the bulky POM anions efficiently inhibit detrimental intermolecular π–π stacking between nearest neighboring BODIPY molecules which mainly interact via C-H···F and C-H···π hydrogen-bonds. However, POMs do not act only as simple molecular spacers, and their negative charge density[45] is also a key factor to drive the supramolecular arrangements of $\mathbf{1}^+$. Thus, when associated with $[W_6O_{19}]^{2-}$ which has a low negative charge density, $\mathbf{1}^+$ forms isolated head-to-tail dimers in both $\mathbf{(1)_2[W_6O_{19}]\cdot 2CH_3CN}$ and $\mathbf{(1)_2[W_6O_{19}]}$.

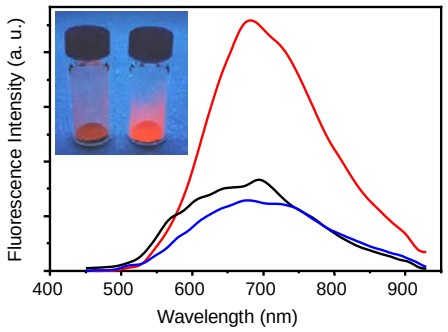

Figure 6. Room-temperature PL spectra of $(\mathbf{1})_2[W_6O_{19}]\cdot 2CH_3CN$ (blue line), $(\mathbf{1})_2[W_6O_{19}]$ (black line) and $(\mathbf{1})_4[Mo_8O_{26}]\cdot DMF\cdot H_2O$ (red line) monitored at λ_{ex} = 365 nm. Inset: photograph of crystalline powders of **(1)Br** (left) and $(\mathbf{1})_4[Mo_8O_{26}]\cdot DMF\cdot H_2O$ (right) under illumination at 365 nm.

In contrast, β-$[Mo_8O_{26}]^{4-}$ has a negative charge density higher than $[W_6O_{19}]^{2-}$ and it interacts more strongly with $\mathbf{1}^+$ cations, increasing their volume concentration in the crystal lattice. This significantly impacts the PL properties. Indeed, the emissions of $(\mathbf{1})_2[W_6O_{19}]\cdot 2CH_3CN$, $(\mathbf{1})_2[W_6O_{19}]$ and $(\mathbf{1})_4[Mo_8O_{26}]\cdot DMF\cdot H_2O$ are characterized by the CIE chromaticity coordinates of (0.55, 0.43), (0.58, 0.41) and (0.62, 0.38), respectively (Figure S16) which results in a progressive red-shift of the emission color. However, comparing the three hybrid POMs of this series, it appears that the higher the $\mathbf{1}^+$ volume concentration, the brighter the fluorescence. Considering that $(\mathbf{1})_2[W_6O_{19}]\cdot 2CH_3CN$ and $(\mathbf{1})_2[W_6O_{19}]$ exhibit comparable weak fluorescence, we may assume that the molecular arrangement of $\mathbf{1}^+$ into head-to-tail dimers should dramatically favor self-quenching processes. The improved PL performances of $(\mathbf{1})_4[Mo_8O_{26}]\cdot DMF\cdot H_2O$ could be possibly attributed to the effect of the β-$[Mo_8O_{26}]^{4-}$ unit on the cationic BODIPY arrangement which results in the absence of the undesirable dimeric stacking and in an increase of the shortest distance between the boradiazaindacene planes of nearest luminophores.

CONCLUSION

$(\mathbf{1})_2[W_6O_{19}]\cdot 2CH_3CN$, $(\mathbf{1})_2[W_6O_{19}]$ and $(\mathbf{1})_4[Mo_8O_{26}]\cdot DMF\cdot H_2O$ represent very rare examples of crystallized hybrid compounds with a fluorescent cationic BODIPY ($\mathbf{1}^+$) derivative. The three structurally resolved supramolecular assemblies combine the $\mathbf{1}^+$ molecule with two different POM anions. Importantly, in addition to their crucial structural role, the β-$[Mo_8O_{26}]^{4-}$ and $[W_6O_{19}]^{2-}$ polyanions were properly chosen as these poor electron acceptors exhibit high energy LMCT transitions in the 250-300 nm range, and they do not compete with $\mathbf{1}^+$ upon photoexcitation at 365 nm. As anticipated, the in-depth structural investigation points out that the bulky POM anions prevent detrimental π–π stacking interactions between the BODIPY cations, which could have resulted in undesired ACQ effect. Moreover, the coupling of $\mathbf{1}^+$ with POMs via non-covalent interactions significantly modifies its fluorescence in the crystalline state, and the three ionic assemblies exhibit contrasted colors and brightnesses which vary with the nature of the POMs and the design of the framework. The assembly of $\mathbf{1}^+$ with $[W_6O_{19}]^{2-}$ having a low negative charge density favors the organization of $\mathbf{1}^+$ into supramolecular dimers in $(\mathbf{1})_2[W_6O_{19}]\cdot 2CH_3CN$ and $(\mathbf{1})_2[W_6O_{19}]$, affording weak fluorescence. In strong contrast in $(\mathbf{1})_4[Mo_8O_{26}]\cdot DMF\cdot H_2O$, the association of $\mathbf{1}^+$ with β-$[Mo_8O_{26}]^{4-}$ which has a higher negative charge density induces a higher volume concentration in BODIPY cations while avoiding its dimeric arrangement, that leads to an intense emission at room temperature. This can be tentatively explained by the existence of weaker interactions between the cationic fluorophores in this compound compared to those found in the Lindqvist ones, these last exhibiting shorter centre-to-centre distances between the neighboring indacene planes. This simple strategy of assembling then sounds promising to improve PL performances of BODIPY entities in the solid state, as long as limiting the choice of POMs to poor electron acceptors to avoid photo-induced electron transfer processes likely to cause the luminescence quenching of organic emitter. As such POMs offer a large diversity of size and charge, this work paves the way towards the design of new ionic assemblies with a high degree of organization, and will allow deeper investigating the precise impact of the POMs on the photophysical properties of cationic BODIPY derivatives in the crystalline state.

ASSOCIATED CONTENT

Supporting Information

Physical measurements, experimental section, ^{1}H NMR spectra, ES/MS spectrum, TGA curve, crystallographic data, FT-IR and UV-vis spectra, 2D photoluminescence excitation-emission map, CIE chromaticity diagrams, luminescence decay curves and extracted lifetimes. This material is available free of charge via the Internet at http://pubs.acs.org.

AUTHOR INFORMATION

Corresponding Author

*E-mail: remi.dessapt@cnrs-imn.fr
*E-mail: olivier.oms@uvsq.fr

ORCID

Rémi Dessapt: 0000-0002-2862-7767
Olivier Oms: 0000-0002-0745-1651
Eric Faulques: 0000-0002-7761-8509
Hélène Serier-Brault: 0000-0002-3300-1347
Anne Dolbecq: 0000-0001-7940-4152
Jérome Marrot: 0000-0002-5351-4908
Pierre Mialane: 0000-0002-8519-7943

NOTES

The authors declare no competing financial interests.

ACKNOWLEDGMENT

Aurélie Damond is gratefully acknowledged for performing mass spectroscopy analysis. This work was supported by the Ministère de l'Enseignement Supérieur et de la Recherche, the CNRS, the Université de Versailles Saint Quentin en Yvelines, the Université de Nantes, the LUMOMAT project supported by the Région des Pays de la Loire and a public grant overseen by the French National Research Agency (ANR) as part of the

"Investissements d'Avenir" program n°ANR-11-IDEX-0003-02 and CHARMMMAT ANR-11-LABX-0039.

REFERENCES

(1) Ostroverkhova, O. Organic Optoelectronic Materials: Mechanisms and Applications. *Chem. Rev.* **2016**, *116*, 13279–13412.

(2) Huang, H.; Yu, Z.; Zhou, D.; Li, S.; Fu, L.; Wu, Y.; Gu, C.; Liao, Q.; Fu, H. Wavelength-Turnable Organic Microring Laser Arrays from Thermally Activated Delayed Fluorescent Emitters. *ACS Photonics* **2019**, *6*, 3208–3214.

(3) Bunzmann, N.; Weissenseel, S.; Kudriashova, L.; Gruene, J.; Krugmann, B.; Grazulevicius, J. V.; Sperlich, A.; Dyakonov, V. Optically and Electrically Excited Intermediate Electronic States in Donor:Acceptor Based OLEDs. *Mater. Horiz.* **2020**, *7*, 1126–1137.

(4) Ni, F.; Li, N.; Zhan, L.; Yang, C. Organic Thermally Activated Delayed Fluorescence Materials for Time-Resolved Luminescence Imaging and Sensing. *Adv. Opt. Mater.* **2020**, *8*, 1902187.

(5) Cheng, H.-B.; Li, Y.; Tang, B. Z.; Yoon, J. Assembly Strategies of Organic-Based Imaging Agents for Fluorescence and Photoacoustic Bioimaging Applications. *Chem. Soc. Rev.* **2020**, *49*, 21–31.

(6) Yuan, J.; Christensen, P. R.; Wolf, M. O. Dynamic Anti-Counterfeiting Security Features Using Multicolor Dianthryl Sulfoxides. *Chem. Sci.* **2019**, *10*, 10113–10121.

(7) Loudet, A.; Burgess, K. BODIPY Dyes and Their Derivatives: Syntheses and Spectroscopic Properties. *Chem. Rev.* **2007**, *107*, 4891–4932.

(8) Zhang, D.; Wen, Y.; Xiao, Y.; Yu, G.; Liu, Y.; Qian, X. Bulky 4-Tritylphenylethynyl Substituted Boradiazaindacene: Pure Red Emission, Relatively Large Stokes Shift and Inhibition of Self-Quenching. *Chem. Commun.* **2008**, 39, 4777–4779.

(9) Vu, T. T.; Badré, S.; Dumas-Verdes, C.; Vachon, J.-J.; Julien, C.; Audebert, P.; Senotrusova, E. Yu.; Schmidt, E. Yu.; Trofimov, B. A.; Pansu, R. B.; Clavier, G.; Méallet-Renault, R. New Hindered BODIPY Derivatives: Solution and Amorphous State Fluorescence Properties. *J. Phys. Chem. C* **2009**, *113*, 11844–11855.

(10) Lu, H.; Wang, Q.; Gai, L.; Li, Z.; Deng, Y.; Xiao, X.; Lai, G.; Shen, Z. Tuning the Solid-State Luminescence of BODIPY Derivatives with Bulky Arylsilyl Groups: Synthesis and Spectroscopic Properties. *Chem. – Eur. J.* **2012**, *18*, 7852–7861.

(11) Sirbu, D.; Benniston, A. C.; Harriman, A. One-Pot Synthesis of a Mono-O,B,N-Strapped BODIPY Derivative Displaying Bright Fluorescence in the Solid State. *Org. Lett.* **2017**, *19*, 1626–1629.

(12) Kim, S.; Bouffard, J.; Kim, Y. Tailoring the Solid-State Fluorescence Emission of BODIPY Dyes by Meso Substitution. *Chem. – Eur. J.* **2015**, *21*, 17459–17465.

(13) Zhang, S.; Wang, Y.; Meng, F.; Dai, C.; Cheng, Y.; Zhu, C. Circularly Polarized Luminescence of AIE-Active Chiral O-BODIPYs Induced via Intramolecular Energy Transfer. *Chem. Commun.* **2015**, *51*, 9014–9017.

(14) Hu, R.; Lager, E.; Aguilar-Aguilar, A.; Liu, J.; Lam, J. W. Y.; Sung, H. H. Y.; Williams, I. D.; Zhong, Y.; Wong, K. S.; Peña-Cabrera, E.; Tang, B. Z. Twisted Intramolecular Charge Transfer and Aggregation-Induced Emission of BODIPY Derivatives. *J. Phys. Chem. C* **2009**, *113*, 15845–15853.

(15) Singh, R. S.; Kumar, A.; Mukhopadhyay, S.; Sharma, G.; Koch, B.; Pandey, D. S. An Unconventional Mechanistic Insight on Aggregation Induced Emission in Novel Boron Dipyrromethenes and Their Rational Biological Realizations. *J. Phys. Chem. C* **2016**, *120*, 22605–22614.

(16) Mukherjee, S.; Thilagar, P. Fine-Tuning Dual Emission and Aggregation-Induced Emission Switching in NPI–BODIPY Dyads. *Chem. – Eur. J.* **2014**, *20*, 9052–9062.

(17) Liu, Z.; Jiang, Z.; Yan, M.; Wang, X. Recent Progress of BODIPY Dyes With Aggregation-Induced Emission. *Front. Chem.* **2019**, *7*, 712.

(18) Yeo, H.; Tanaka, K.; Chujo, Y. Effective Light-Harvesting Antennae Based on BODIPY-Tethered Cardo Polyfluorenes via Rapid Energy Transferring and Low Concentration Quenching. *Macromolecules* **2013**, *46*, 2599–2605.

(19) Zhu, M.; Jiang, L.; Yuan, M.; Liu, X.; Ouyang, C.; Zheng, H.; Yin, X.; Zuo, Z.; Liu, H.; Li, Y. Efficient Tuning Nonlinear Optical Properties: Synthesis and Characterization of a Series of Novel Poly(Aryleneethynylene)s Co-Containing BODIPY. *J. Polym. Sci. Part Polym. Chem.* **2008**, *46*, 7401–7410.

(20) Liras, M.; Iglesias, M.; Sánchez, F. Conjugated Microporous Polymers Incorporating BODIPY Moieties as Light-Emitting Materials and Recyclable Visible-Light Photocatalysts. *Macromolecules* **2016**, *49*, 1666–1673.

(21) Glembockyte, V.; Frenette, M.; Mottillo, C.; Durantini, A. M.; Gostick, J.; Štrukil, V.; Friščić, T.; Cosa, G. Highly Photostable and Fluorescent Microporous Solids Prepared via Solid-State Entrapment of Boron Dipyrromethene Dyes in a Nascent Metal–Organic Framework. *J. Am. Chem. Soc.* **2018**, *140*, 16882–16887.

(22) Wang, S.-S.; Yang, G.-Y. Recent Advances in Polyoxometalate-Catalyzed Reactions. *Chem. Rev.* **2015**, *115*, 4893–4962.

(23) Du, D.-Y.; Qin, J.-S.; Li, S.-L.; Su, Z.-M.; Lan, Y.-Q. Recent Advances in Porous Polyoxometalate-Based Metal–Organic Framework Materials. *Chem. Soc. Rev.* **2014**, *43*, 4615–4632.

(24) Proust, A.; Matt, B.; Villanneau, R.; Guillemot, G.; Gouzerh, P.; Izzet, G. Functionalization and Post-Functionalization: A Step towards Polyoxometalate-Based Materials. *Chem. Soc. Rev.* **2012**, *41*, 7605–7622.

(25) Dridi, H.; Boulmier, A.; Bolle, P.; Dolbecq, A.; Rebilly, J.-N.; Banse, F.; Ruhlmann, L.; Serier-Brault, H.; Dessapt, R.; Mialane, P.; Oms, O. Directing the Solid-State Photochromic and Luminescent Behaviors of Spiromolecules with Dawson and Anderson Polyoxometalate Units. *J. Mater. Chem. C* **2020**, *8*, 637–649.

(26) Oms, O.; Hakouk, K.; Dessapt, R.; Deniard, P.; Jobic, S.; Dolbecq, A.; Palacin, T.; Nadjo, L.; Keita, B.; Marrot, J.; Mialane, P. Photo- and Electrochromic Properties of Covalently Connected Symmetrical and Unsymmetrical Spiropyran–Polyoxometalate Dyads. *Chem. Commun.* **2012**, *48*, 12103–12105.

(27) Saad, A.; Oms, O.; Marrot, J.; Dolbecq, A.; Hakouk, K.; El Bekkachi, H.; Jobic, S.; Deniard, P.; Dessapt, R.; Garrot, D.; Boukheddaden, K.; Liu, R.; Zhang, G.; Keita, B.; Mialane, P. Design and Optical Investigations of a Spironaphthoxazine/Polyoxometalate/Spiropyran Triad. *J. Mater. Chem. C* **2014**, *2*, 4748–4758.

(28) Hakouk, K.; Oms, O.; Dolbecq, A.; Marrot, J.; Saad, A.; Mialane, P.; El Bekkachi, H.; Jobic, S.; Deniard, P.; Dessapt, R. New Photoresponsive Charge-Transfer Spiropyran/Polyoxometalate Assemblies with Highly Tunable Optical Properties. *J. Mater. Chem. C* **2014**, *2*, 1628–1641.

(29) Menet, C.; Serier-Brault, H.; Oms, O.; Dolbecq, A.; Marrot, J.; Saad, A.; Mialane, P.; Jobic, S.; Deniard, P.; Dessapt, R. Influence of Electronic vs. Steric Factors on the Solid-State Photochromic Performances of New Polyoxometalate/Spirooxazine and Spiropyran Hybrid Materials. *RSC Adv.* **2015**, *5*, 79635–79643.

(30) Bolle, P.; Serier-Brault, H.; Génois, R.; Faulques, E.; Boulmier, A.; Oms, O.; Lepeltier, M.; Marrot, J.; Dolbecq, A.; Mialane, P.; Dessapt, R. Drastic Solid-State Luminescence Color Tuning of an Archetypal Ir(Iii) Complex Using Polyoxometalates and Its Application as a Vapoluminescence Chemosensor. *J. Mater. Chem. C* **2016**, *4*, 11392–11395.

(31) Bolle, P.; Serier-Brault, H.; Boulmier, A.; Puget, M.; Menet, C.; Oms, O.; Marrot, J.; Mialane, P.; Dolbecq, A.; Dessapt, R. Polymorphism and Structural Filiations in Five New Organic–Inorganic Hybrid Salts of the Heteroleptic Cationic Iridium(III) Complex and Polyoxometalates. *Cryst. Growth Des.* **2018**, *18*, 7426–7434.

(32) Bolle, P.; Chéret, Y.; Roiland, C.; Sanguinet, L.; Faulques, E.; Serier-Brault, H.; Bouit, P.-A.; Hissler, M.; Dessapt, R. Strong Solid-State Luminescence Enhancement in Supramolecular Assemblies of Polyoxometalate and "Aggregation-Induced Emission"-Active Phospholium. *Chem. – Asian J.* **2019**, *14*, 1642–1646.

(33) Black, F. A.; Jacquart, A.; Toupalas, G.; Alves, S.; Proust, A.; Clark, I. P.; Gibson, E. A.; Izzet, G. Rapid Photoinduced Charge Injection into Covalent Polyoxometalate–Bodipy Conjugates. *Chem. Sci.* **2018**, *9*, 5578–5584.

(34) Saad, A.; Oms, O.; Dolbecq, A.; Menet, C.; Dessapt, R.; Serier-Brault, H.; Allard, E.; Baczko, K.; Mialane, P. A High Fatigue Resistant, Photoswitchable Fluorescent Spiropyran–Polyoxometalate–BODIPY Single-Molecule. *Chem. Commun.* **2015**, *51*, 16088–16091.

(35) Benazzi, E.; Karlsson, J.; M'Barek, Y. B.; Chabera, P.; Blanchard, S.; Alves, S.; Proust, A.; Pullerits, T.; Izzet, G.; Gibson, E. Acid-Triggering of Light-Induced Charge-Separation in

Hybrid Organic/Inorganic Molecular Photoactive Dyads for Harnessing Solar Energy. *Inorg. Chem. Front.* **2021,** *8*, 1610-1618.

(36) Toupalas, G.; Karlsson, J.; Black, F. A.; Masip-Sánchez, A.; López, X.; M'Barek, Y. B.; Blanchard, S.; Proust, A.; Alves, S.; Chabera, P.; Clark, I. P.; Pullerits, T.; Poblet, J. M.; Gibson, E. A.; Izzet, G. Tuning Photoinduced Electron Transfer in POM-Bodipy Hybrids by Controlling the Environment: Experiment and Theory. *Angew. Chem. Int. Ed.* **2021**, *60*, 6518-6525.

(37) Gu, Y.; Li, Q.; Huang, Y.; Zhu, Y.; Wei, Y.; Ruhlmann, L. Polyoxovanadate-Iodobodipy Supramolecular Assemblies: New Agents for High Efficiency Cancer Photochemotherapy. *Chem. Commun.* **2020**, *56*, 2869–2872.

(38) Kim, T.-I.; Park, J.; Kim, Y. A Gold Nanoparticle-Based Fluorescence Turn-On Probe for Highly Sensitive Detection of Polyamines. *Chem. – Eur. J.* **2011**, *17*, 11978–11982.

(39) Klemperer, W. G. Tetrabutylammonium Isopolyoxometalates. In *Inorganic Syntheses*; John Wiley & Sons, Ltd, 1990; 74–85.

(40) Sanchez, C.; Livage, J.; Launay, J. P.; Fournier, M. Electron Delocalization in Mixed-Valence Tungsten Polyanions. *J. Am. Chem. Soc.* **1983**, *105*, 6817–6823.

(41) Hakouk, K.; Oms, O.; Dolbecq, A.; El Moll, H.; Marrot, J.; Evain, M.; Molton, F.; Duboc, C.; Deniard, P.; Jobic, S.; Mialane, P.; Dessapt, R. Sulfonium Polyoxometalates: A New Class of Solid-State Photochromic Hybrid Organic–Inorganic Materials. *Inorg. Chem.* **2013**, *52*, 555–557.

(42) Liu, C.-L.; Chen, Y.; Shelar, D. P.; Li, C.; Cheng, G.; Fu, W.-F. Bodipy Dyes Bearing Oligo(Ethylene Glycol) Groups on the Meso-Phenyl Ring: Tuneable Solid-State Photoluminescence and Highly Efficient OLEDs. *J. Mater. Chem. C* **2014**, *2*, 5471–5478.

(43) Tian, D.; Qi, F.; Ma, H.; Wang, X.; Pan, Y.; Chen, R.; Shen, Z.; Liu, Z.; Huang, L.; Huang, W. Domino-like multi-emissions across red and near infrared from solid-state 2-/2,6-aryl substituted BODIPY dyes. *Nat. Commun.* **201**8, 9, 2688 (10.1038/s41467-018-05040-8).

(44) Duan, C.; Zhou, Y.; Shan, G.-G.; Chen, Y.; Zhao, W.; Yuan, D.; Zeng, L.; Huang, X.; Niu, G. Bright solid-state red-emissive BODIPYs: facile synthesis and their high-contrast mechanochromic properties. *J. Mater. Chem. C* **2019**, *7*, 3471–3478.

(45) Misra, A.; Kozma, K.; Streb, C.; Nyman, M. Beyond Charge Balance: Counter-Cations in Polyoxometalate Chemistry. *Angew. Chem. Int. Ed.* **2020**, *59*, 596–612.